Enhanced climate response to ozone depletion from ozone-circulation coupling

Pu Lin[1] and Yi Ming[2]

[1]Princeton University
[2]Geophysical Fluid Dynamics Laboratory

November 23, 2022

Abstract

The effect of stratospheric ozone depletion is simulated in GFDL AM4 model with three ozone schemes: prescribing monthly zonal mean ozone concentration, full interactive stratospheric chemistry, and a simplified linear ozone chemistry scheme but with full dynamical interactions. While similar amounts of ozone loss are simulated by the three schemes, the two interactive ozone schemes produce significantly stronger stratospheric cooling than the prescribed one. We find that this temperature difference is driven by the dynamical responses to ozone depletion. In particular, the existence of ozone hole leads to strong ozone eddies that are in-phase with the temperature eddies. The coherence between ozone and temperature anomalies leads to a weaker radiative damping as ozone absorbs shortwave radiation that compensates for the longwave cooling. As a result, less wave dissipates at the lower stratosphere, leading to a weaker descending and dynamical heating over the polar lower stratosphere, and hence a stronger net cooling there. The covariance between ozone and temperature is largely suppressed when ozone is prescribed as monthly zonal mean time series, as is the reduction in the radiative damping following ozone depletion. With much lower computational cost, the simplified ozone scheme is capable of producing similar magnitude of ozone loss and the consequent dynamical responses to those simulated by the full chemistry.

Enhanced climate response to ozone depletion from ozone-circulation coupling

Pu Lin[1,2], **and Yi Ming** [2]

[1]Program in Atmospheric and Oceanic Sciences, Princeton University, Princeton, NJ

[2]NOAA/Geophysical Fluid Dynamics Laboratory

Key Points:

- Interactive ozone schemes produce stronger stratospheric cooling than prescribing the same ozone changes.
- Dynamical response to ozone depletion drives the difference in temperature response.
- A cheap interactive ozone scheme is developed and behaves similarly to the full chemistry scheme.

Corresponding author: Pu Lin, `pulin@princeton.edu`

Abstract

The effect of stratospheric ozone depletion is simulated in GFDL AM4 model with three ozone schemes: prescribing monthly zonal mean ozone concentration, full interactive stratospheric chemistry, and a simplified linear ozone chemistry scheme but with full dynamical interactions. While similar amounts of ozone loss are simulated by the three schemes, the two interactive ozone schemes produce significantly stronger stratospheric cooling than the prescribed one. We find that this temperature difference is driven by the dynamical responses to ozone depletion. In particular, the existence of ozone hole leads to strong ozone eddies that are in-phase with the temperature eddies. The coherence between ozone and temperature anomalies leads to a weaker radiative damping as ozone absorbs shortwave radiation that compensates for the longwave cooling. As a result, less wave dissipates at the lower stratosphere, leading to a weaker descending and dynamical heating over the polar lower stratosphere, and hence a stronger net cooling there. The covariance between ozone and temperature is largely suppressed when ozone is prescribed as monthly zonal mean time series, as is the reduction in the radiative damping following ozone depletion. With much lower computational cost, the simplified ozone scheme is capable of producing similar magnitude of ozone loss and the consequent dynamical responses to those simulated by the full chemistry.

Plain Language Summary

It is well-known that the ozone hole over Antarctica leads to a strong cooling in the stratosphere. However, when simulating this effect in climate models, we find that the magnitude of the cooling depends on how ozone is represented in the model. Compared to the model specifying ozone concentrations as monthly time series, stronger cooling is found in the model calculating ozone concentrations from the photochemical reactions. This is because the spatial distribution and the short-term temporal variation of ozone are not consistent with the circulation when ozone is specified, which leads to a stronger over-turning circulation with ascending branch over the tropics and descending branch over the polar region. The stronger descending motion then drives a stronger dynamical heating that compensates for the radiative cooling induced by ozone loss. As a result, a weaker net cooling is produced in the model with specified ozone. We also test a model in which ozone is allowed to vary with the circulation, but the chemical processes are greatly simplified. The computational cost of this model is much cheaper than the

one that incorporates the photochemical reactions, but the magnitude of the simulated stratospheric cooling is similar.

1 Introduction

Stratospheric ozone changes impose a significant forcing to the climate system. The depletion of stratospheric ozone occurring over the past few decades has been credited with being a major driver for circulation changes, especially over the Southern Hemisphere (Solomon, 1999; Polvani et al., 2011). Despite its importance, most climate models do not simulate the chemical reactions producing and depleting ozone, but prescribe monthly time series of ozone concentration instead (Eyring et al., 2013; Gerber & Son, 2014; Checa-Garcia et al., 2018; Keeble et al., 2020). Computational cost is a major hurdle for climate models to include full stratosphere chemistry.

While the radiative cooling in the stratosphere is certainly the leading effect of ozone depletion, it has long been suspected that there may be non-trivial chemical and dynamical feedbacks to ozone changes that are not represented by prescribing monthly ozone time series. This motivates comparisons between the models participating the Coupled Model Intercomparison Project (CMIP) phase 3 and 5 and the chemistry climate models which incorporate fully interactive ozone. The multi-model means of the two groups do not always show a clear distinction in terms of responses to ozone depletion (Son et al., 2008, 2010; Gerber & Son, 2014), which may not be surprising given the large structural difference among models. A more appropriate comparison would be utilizing a single model where the only change between simulations is how ozone is represented. Such single model studies show that the interactive ozone leads to stronger response to ozone depletion in the Southern Hemisphere (Gillett et al., 2009; Waugh et al., 2009; Neely et al., 2014; Li et al., 2016; Haase et al., 2020), and stronger variability in the Northern Hemisphere polar region (Haase & Matthes, 2019; Rieder et al., 2019).

It is important to recognize that prescribing ozone not only ignores the interaction between the chemical reactions and the background meteorological conditions, but also suppresses the coupling between ozone and circulation. Earlier studies have attributed the difference between the simulations with and without full chemistry to the zonal asymmetry in the ozone concentration (Gillett et al., 2009; Waugh et al., 2009). This motivated CMIP6 models to specify longitudinally-varying ozone instead of zonal mean (Checa-

Garcia et al., 2018; Keeble et al., 2020). Rae et al. (2019) further proposed a scheme to redistribute ozone according to the potential vorticity (PV) field. This inexpensive modification brings about an ozone field that is more consistent with the dynamics, and is found to greatly ease the bias in the Northern Hemisphere, but is not helpful and even causes stronger bias in the Southern Hemisphere (Rae et al., 2019). A recent study by Neely et al. (2014) showed that specifying monthly mean ozone concentrations effectively dampens the temporal variation, leading to significantly weaker ozone loss realized by the model. They hence proposed to prescribe daily zonal mean ozone instead of monthly mean.

In this study, we revisit the issue of how ozone depletion affects the climate system using the GFDL AM4 model (Zhao et al., 2018a, 2018b). We compare the simulations of AM4 with full stratospheric chemistry against the ones with specified monthly zonal mean ozone concentrations. In addition, we introduce a new scheme to represent ozone variations in the model, which is computationally as cheap as specifying ozone. We find that specifying monthly zonal mean ozone underestimates the effect of ozone depletion, but the new scheme can reproduce the magnitude of the springtime stratospheric cooling simulated in the full chemistry simulations. The physical process leading to the biases in prescribing monthly zonal mean ozone is identified and assessed. In the following, we will first give a detailed description of the simulations in section 2, then the results are presented in section 3, which is followed by a summary and discussion in section 4.

2 Model and Experiments

In this study, we employ the GFDL AM4 (Zhao et al., 2018a, 2018b), the atmospheric component of the GFDL's coupled physical model CM4 (Held et al., 2019). We follow the model configuration documented by Zhao et al. (2018b) except that the model top is raised from 1 hPa to 0.01 hPa, and the vertical resolution is increased from 33 levels to 63 levels. This is to ensure sufficient resolution to resolve the stratosphere. Despite the difference in the model top and the vertical coordinate, the simulated troposphere and surface climate are generally similar to those reported by Zhao et al. (2018a).

The default AM4 consists of a light tropospheric chemistry scheme and prescribes monthly zonal mean ozone concentration. Simulations with this setting are referred to as control (CNTL) in this study. We also perform simulations with fully interactive chemistry (FullChem) using the chemistry scheme as in the GFDL earth system model ESM4 (Dunne et al., 2020) and AM4.1 (Horowitz et al., 2020). The stratospheric chemistry formulation and its performance is documented by Austin and Wilson (2006).

In addition, we designe a simplified ozone scheme, in which ozone is treated as a tracer in the model that can be freely transported by circulation as in FullChem, but the chemical tendency of the tracer is reduced to the following:

$$\left.\frac{D[O3]}{Dt}\right|_{chem} = P - \frac{[O3]}{\tau} \tag{1}$$

where $[O3]$ is the ozone concentration, P is the chemical production rate of ozone, and τ is the chemical lifetime. Derivation and samples of P and τ are given in the Appendix. Both P and τ are specified in the model as monthly zonal mean time series. This scheme thus allows full dynamical interaction between ozone and circulation while restraining the chemical interactions. Simulations with this ozone scheme are referred to as O3Tracer.

There have been several simplified stratospheric ozone schemes that specify the chemical tendency as a linear function of ozone concentration, temperature and partial column of ozone, with additional terms to account for the heterogeneous reactions (e.g., Cariolle & Déqué, 1986; McLinden et al., 2000; McCormack et al., 2004). These linear schemes are widely used in the numerical weather models that have more stringent constraints on computational cost. The application of the linear ozone scheme to the climate models are much rarer, with noticeable exceptions of the climate models from CNRM (Voldoire et al., 2013; Michou et al., 2019) and the recent E3SM (Golaz et al., 2019). The coefficients are usually derived from an off-line chemistry model specified with a certain meteorological state, and often lead to spurious results for the severe ozone depletion over the Antarctica that are highly nonlinear (Geer et al., 2007; Monge-Sanz et al., 2011; Eyring et al., 2013). To some extent, our O3Tracer scheme is a simplified version of these linear ozone schemes. However, by prescribing different P and τ for different climate states, all the chemical changes are factored in regardless whether they are linear or nonlinear with respect to the meteorological states. As will be shown below, the two terms in Eq. 1 are sufficient to capture the bulk of ozone loss.

We conduct a pair of time-slice experiments with each ozone schemes: *1960O3* and *2010O3*. For FullChem, ozone depleting substances are set to either year 1960 or 2010 level, corresponding to the unperturbed and depleted states, respectively. The CNTL and O3Tracer simulations then take the monthly zonal mean climatology from the corresponding FullChem simulations. All other forcings and SST/SICs are set to year 2010 level, and are identical in all simulations. Each simulation is run for 80 years, and the first 10 years are considered as the spin-up and discarded. Most analyses are focused in the lower stratosphere over the Southern Hemisphere polar region, where the ozone depletion is the severest.

In addition, we use the Fu-Liou radiative transfer model (Fu & Liou, 1992; Rose & Charlock, 2002) to calculate the radiative effect of ozone changes. The off-line radiative transfer calculation assumes clean-sky condition (i.e., no clouds or aerosols), and uses November mean zonal mean profiles of temperature, ozone, and water vapor concentration, and surface albedo from the corresponding simulations. The calculation uses the four-stream algorithm, and a one-day calculation is done for 16 November. Note that this is not the radiative transfer model used in AM4, but the difference due to radiative schemes is generally small. In general, Fu-Liou radiative transfer model is more expensive and more accurate than those used in GCMs.

3 Results

We start by comparing the ozone loss and the stratospheric cooling simulated by the three ozone schemes. Figure 1 a and b show the ozone and temperature difference at 100 hPa over the southern polar cap between the *2010O3* and *1960O3* simulations. Reduction of ozone is seen throughout the year with the strongest depletion in October. Consequently, cooling is found over the lower stratospheric polar region, which peaks in November. However, the magnitudes of the cooling among the three simulations are not proportional to their ozone loss. O3Tracer produces weaker ozone loss than the other two. Yet, its resulting cooling is as strong as that in FullChem. It is CNTL that yields the weakest cooling, despite its almost identical ozone loss to FullChem. In November, O3Tracer produces $1.8K$ or 26% more cooling than CNTL, and the difference between Fullchem and CNTL is $2.3K$ or 32%. The difference in the stratospheric cooling between CNTL and the other two are statistically significant at the 95% confidence level.

To interpret this difference in temperature responses, we analyze the heat budget. In the stratosphere, the leading components of the heat budget are the longwave and shortwave radiation as well as dynamical heating, which is brought about by advection of var-

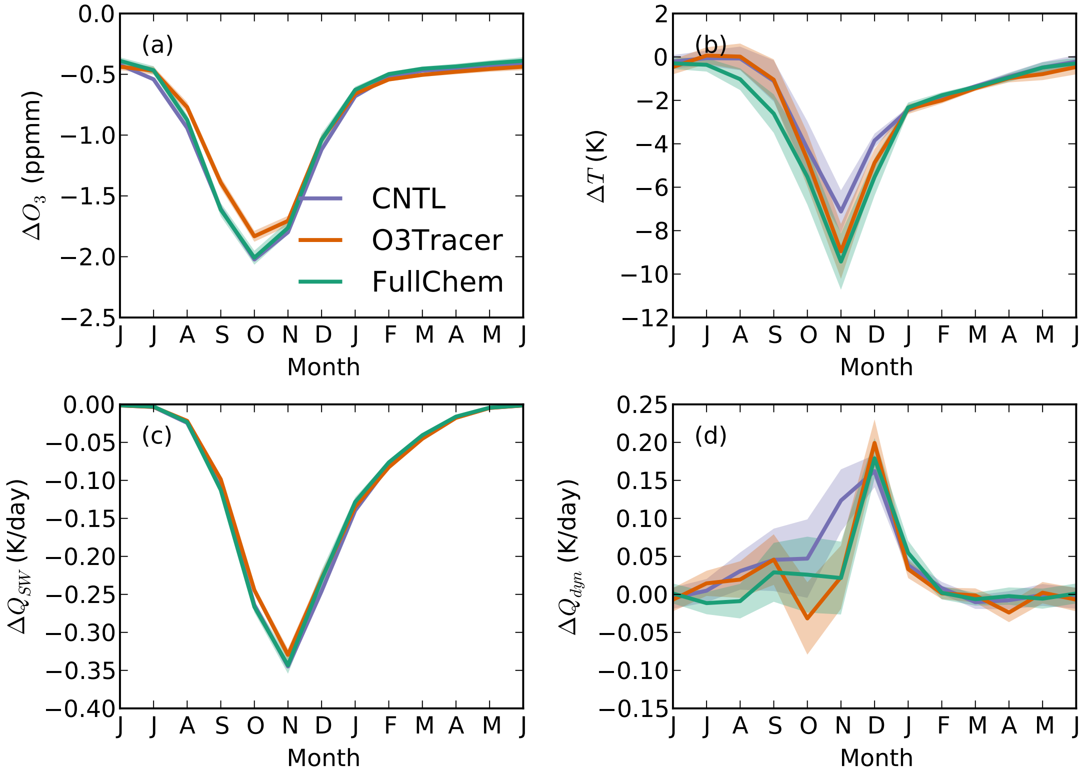

Figure 1. Difference in (a) ozone concentration, (b) temperature, (c) shortwave (SW) heating rate, and (d) dynamical heating rate between the *2010O3* and the *1960O3* experiments. Purple lines are for the CNTL simulation, orange lines are for the O3Tracer simulation, and green lines are for the FullChem simulation. Results are shown at 100 hPa averaged over 60°S and 90°S. Shading indicates the 95% uncertainty range estimated based on the Student's t-test.

ious scales. Following ozone depletion, temperature changes are driven by a reduction of shortwave heating as well as changes in the dynamical heating, whereas longwave radiation largely responds to the temperature variations. As shown in Fig. 1c, similar amounts of decrease in shortwave heating rate are seen among the three simulations. On the other hand, CNTL simulates more dynamical heating than the other two experiments in response to ozone loss (Fig. 1d). The difference in dynamical heating response is most significant in November, when CNTL yields 0.12 K per day more dynamical heating, whereas O3Tracer and FullChem show no significant change. Comparing changes in the radiative and dynamical heating rates, it is clear that the dynamical heating rates drive the diversified temperature responses to ozone depletion in these simulations. Similar results are found at other levels in the lower stratosphere and are not shown.

Focusing on November when the difference in dynamical heating rate and temperature is the largest between CNTL and O3Tracer or FullChem, we investigate the cause of the dynamical heating over the polar stratosphere. The stratosphere is dominated by the Brewer-Dobson circulation (Butchart, 2014, and references therein), an overturning circulation ascending over the low-latitudes and descending over the high-latitudes. An adiabatic warming then results from the descending over the polar region. The strength of the circulation is described by the Transformed Eulerian mean (TEM) velocities, and the dynamical heating rate over the stratospheric polar region is proportional to the TEM vertical velocity w*. Figure 2a plots the TEM vertical velocity w* averaged over the polar region from the three *2010O3* simulations. While all three simulations show descending throughout the stratosphere, the descending in CNTL is stronger than O3Tracer or FullChem in the lower stratosphere, and weaker above.

Because the Brewer-Dobson circulation is a wave-driven circulation, its strength is tightly linked to wave dissipation in the stratosphere. As shown in Fig. 2b, waves typically propagate upward from the troposphere into the stratosphere over mid-latitudes, and dissipate over a broad region over the stratospheric extratropics. Compared to CNTL, both O3Tracer and FullChem show less wave dissipation over the lower half of the stratosphere, and more wave dissipation above (Fig. 2c and 2d). This is consistent with the w* shown in Fig. 2a as downward control principle indicates that w* at a certain level should be proportional to the integrated wave dissipation above that level (Haynes et al., 1991).

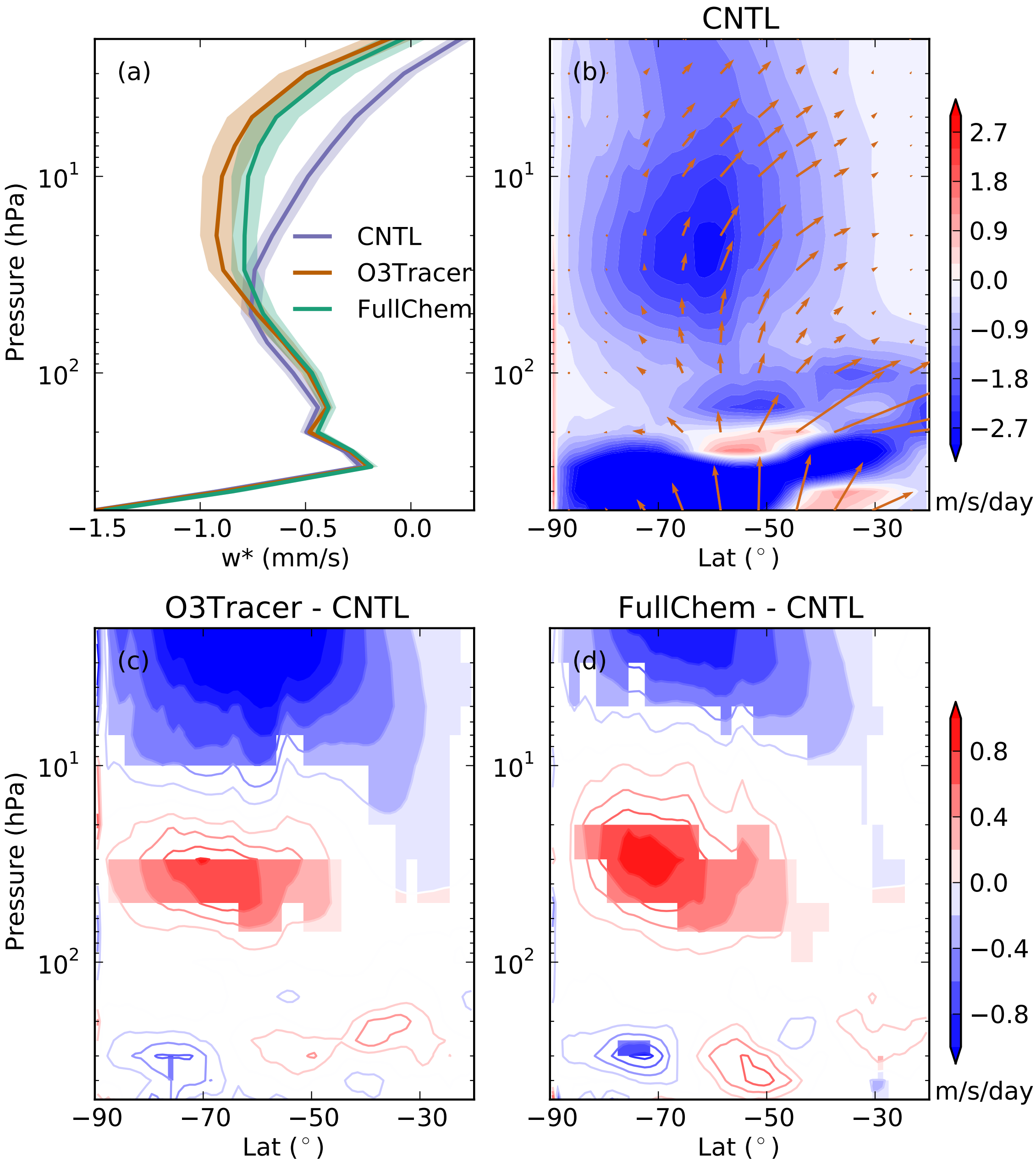

Figure 2. Dynamical conditions in November from the *2010O3* experiment. (a) TEM vertical velocity w* averaged over 60°S-90°S. Shading indicates the 95% uncertainty range estimated based on the Student's t-test. (b) EP flux (vectors) and its divergence (shadings) simulated in the CNTL simulation. (c) Difference in EP flux divergence between the O3Tracer and the CNTL simulations. Contours are filled where the difference is statistically significant at 95% confidence level based on the Student's t-test. (d) As in (c), except for the FullChem simulation. Note that a more negative EP flux divergence indicates more wave dissipation, and vice versa.

A key factor controlling wave propagation and dissipation is the background zonal winds. Linear theory predicts that the upward wave propagation is suppressed when the stratospheric jet is easterly or strong westerly, and strong dissipation occurs when the background zonal wind matches with the phase speed (Charney & Drazin, 1961). Therefore, stronger Brewer-Dobson circulation and stronger dynamical heating over the polar region are expected when the stratospheric jet is moderately westerly. This relationship is confirmed in Fig. 3 which plots the seasonal cycle of the dynamical heating rate and the strength of polar night jet. The *2010O3* experiments show a delayed seasonal cycle in both dynamical heating rates and zonal wind compared to the *1960O3* experiments. But when plotting the dynamical heating rate against the zonal wind, the two experiments share similar characteristics: dynamical heating rate peaks around zonal wind of 20 m/s and diminishes quickly when zonal wind approaches zero as well as increases towards higher values. A secondary peak of dynamical heating rate locates around 10 m/s in austral autumn. The response of dynamical heating to ozone depletion is then explained by zonal winds. Ozone depletion strongly cools the polar stratosphere, which leads to a stronger polar night jet following the thermal wind balance. During late spring/early summer, the wave-wind relationship is in the weak westerly regime, so that a small increase in zonal winds leads to extensive strengthening of the circulation and dynamical warming over the polar region.

However, the difference between CNTL and O3Tracer or FullChem cannot be explained by zonal winds. As shown in Fig. 3c, the *2010O3* simulation with O3Tracer or FullChem shows a weaker dynamical heating than others under the same zonal wind conditions. The disparity is most perceivable when zonal wind is between 20 to 30 m/s, which coincides with November in the *2010O3* simulations. We argue that the responsible process for this difference in the dynamical heating rate and wave dissipation is the radiative damping of the waves.

Radiative damping comes from the basic principle of radiation that a warmer air parcel emits more longwave radiation and hence cools faster, which acts to diminish thermal anomalies. The dissipation from the radiative damping is usually considered as a small term compared to the dissipation induced by zonal winds. However, the zonal wind-induced dissipation is confined to waves of certain phase speed that match with the background zonal winds. The radiative damping, on the other hand, does not have such restriction, and the cumulative effect may not be trivial. Such difference allows us to dis-

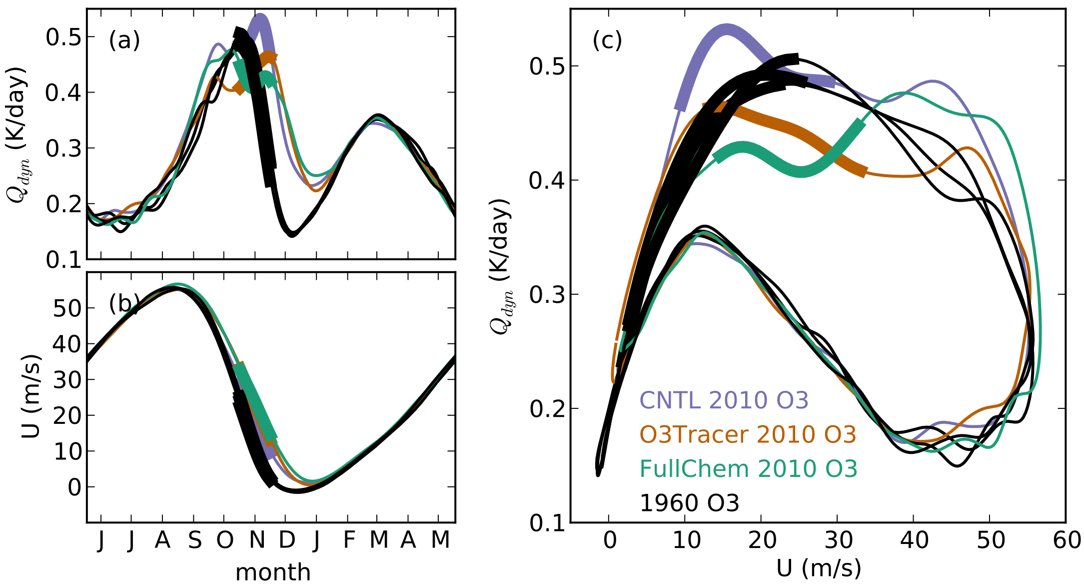

Figure 3. Seasonal cycle of (a) dynamical heating rate at 100 hPa averaged over 60°S-90°S, and (b) zonal mean zonal wind at 50 hPa 60°S. (c) The two seasonal cycle plotted against each other. Seasonal cycles are calculated using daily mean data averaged over the last 70 years of the simulation and then smoothed by a Gaussian kernel with standard deviation of 7 days. November days are marked by the thicker lines. Purple lines are for the CNTL *2010O3* simulations, orange lines are for the O3Tracer *2010O3* simulations, green lines are for the FullChem *2010O3* simulations, and black lines are for the *1960O3* simulations.

tinguish the two types of wave dissipation in the phase speed spectra. Figure 4 shows the difference in wave dissipation between the *2000O3* and the *1960O3* experiments as a function of angular phase speed and latitude in November at 50 Pa. In the CNTL case, less dissipation (positive anomalies) occurs at the lower phase speed, and more dissipation (negative anomalies) occurs at the higher phase speed over high latitudes. Such a shift of wave dissipation towards higher phase speed is consistent with the strengthening of the polar night jet following ozone depletion. This again confirms that the dynamical response to ozone depletion in the CNTL experiment largely comes from the zonal wind-induced wave dissipation.

The changes of wave dissipation simulated from O3Tracer and FullChem (Fig. 4b and 4c) show a more complex pattern than that from CNTL (Fig. 4a). This is because more than one process is at work. We decompose the wave dissipation changes from O3Tracer and FullChem into two components. The first is constructed by subtracting the CNTL *2010O3* wave dissipation spectra from the corresponding O3Tracer and FullChem ones, shown in Figs. 4d and 4e. The second component is simply the residual, shown in Figs. 4f and 4g. We find the second components of O3Tracer and FullChem bear strong similarity to the wave dissipation changes of CNTL, showing wave dissipation shifts towards higher phase speed over high latitudes. The first component, on the other hand, shows an omnipresent reduction of the wave dissipation with a pattern similar to its climatology. We argue that the first component reflects changes in the radiative damping, while the second component is related to the changes in zonal winds.

It is then natural to ask why ozone depletion leads to a weakening of radiative damping in simulations of interactive ozone but not in ones with ozone prescribed. We propose that the weakening of radiative damping comes from the coherence between temperature and ozone anomalies so that warmer air parcel consists of higher ozone concentration. This anomalous ozone absorbs shortwave radiation that partly cancels the longwave cooling, yielding weaker radiative damping.

The coherence between temperature and ozone has been observed as early as the beginning of the satellite era (Newman & Randel, 1988). This is because the long lifetime of ozone in the lower stratosphere makes it a quasi-conservative tracer following the motion of air parcels. Potential temperature and potential vorticity (PV) are also quasi-conservative tracers for motions on timescales of less than a few weeks (Andrews et al.,

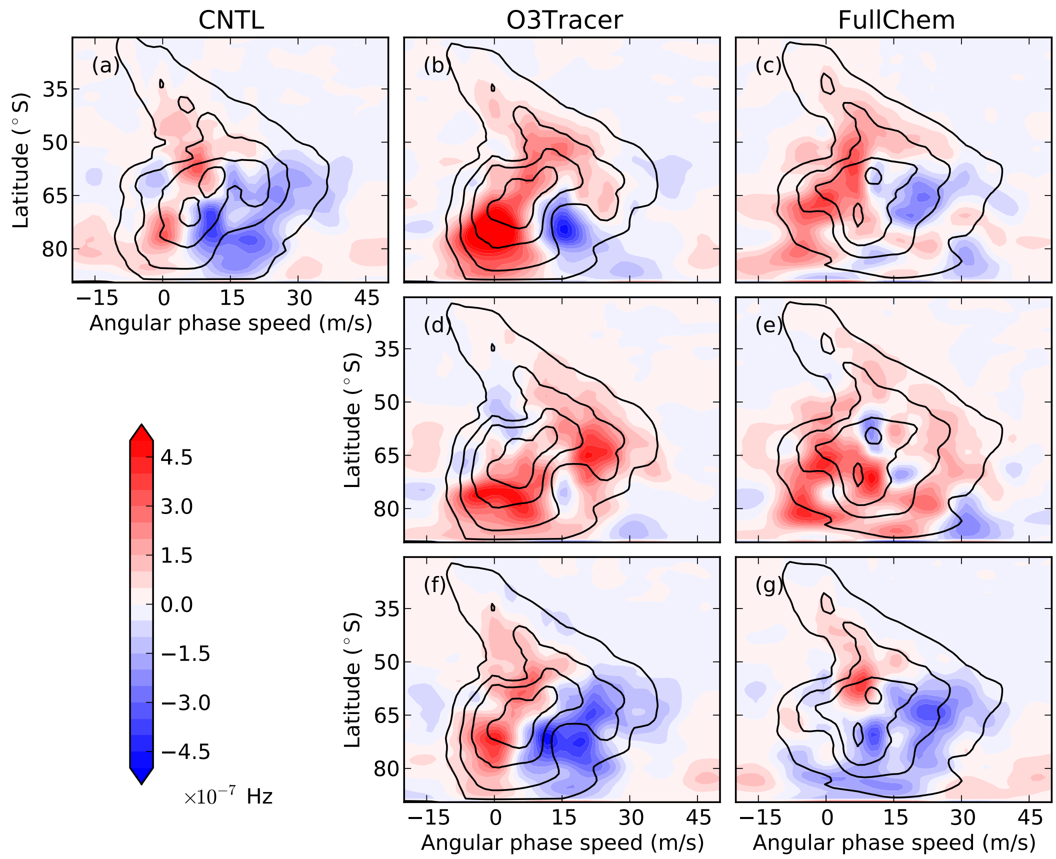

Figure 4. Difference in the phase speed spectra of EP flux divergence at 50 hPa in November between the *2010O3* and the *1960O3* experiments from (a) CNTL, (b) O3Tracer and (c) FullChem simulations. (d) The first component of the spectral responses to ozone depletion simulated in O3Tracer, calculated by subtracting the CNTL *2010O3* from the O3Tracer *2010O3*. (f) The second component of the spectral response to ozone depletion in O3Tracer, calculated as the residual of the first component. (e) and (g) as in (d) and (f), except for the FullChem simulation. Black contours plot the climatology from the *1960O3* experiment at -9, -7, ..., -1 $\times 10^{-7}$ Hz.

1987). Therefore, ozone, temperature and PV are expected to co-vary with each others in the lower stratosphere. As shown in Fig. 5, strong PV gradient is found surrounding the pole, which acts as a barrier between the cold and low-ozone air over the pole and the warm and high-ozone air on the equator side (Schoeberl & Hartmann, 1991). These PV contours never lie perfectly parallel with the latitudinal lines. Instead, they are undergoing constant deformation and displacement while redistributing the air, and hence creating eddies of temperature and ozone along latitudes. Both temperature and ozone anomalies are therefore closely tied to the PV anomalies.

The magnitudes of the ozone and temperature eddies depend on the contrast across the PV gradient barrier. During the ozone depletion era, catalytic reactions occurring on the surface of the polar stratospheric clouds strongly deplete ozone inside the polar vortex (Fig. 5b). During the pre-depletion era, on the other hand, the ozone concentration does not differ much inside and outside the vortex (Fig. 5d). This is not only due to the absence of the catalytic reactions, but also due to the weak vortex in November during the pre-depletion era that are susceptible for air outside the vortex to mix in. Therefore, the same PV perturbation would yield much weaker ozone anomalies in the pre-depletion era. This explains why there is no distinguishable difference in the *1960O3* experiments whether ozone is allowed to interact with circulation or not (black lines in Fig. 3).

The extent of this ozone-circulation interaction depends on the extent of the ozone hole. We therefore expect this interaction has weak effect over low latitudes. The ozone hole is largely confined within the altitudes between 12 and 24 km (Solomon et al., 2005), which is roughly consistent with the weakening of wave dissipation (positive anomalies) shown in Fig. 2c and 2d. The stronger wave dissipation (negative anomalies) seen at the higher levels in Figs. 2c and 2d, on the other hand, is not directly due to the ozone-circulation interaction. Rather, it results from the fact that more waves can reach the upper stratosphere since they are less attenuated at the lower levels. The stronger wave dissipation at the upper stratosphere extends into the low latitudes as the waves turn equator-ward at this altitude (Fig. 2b).

The timing of the ozone-circulation interaction is affected by several factors. Polar vortex needs to be strong enough to hold a severe ozone hole, but also not too strong so that waves can enter the stratosphere and disturb the vortex. At the same time, stronger

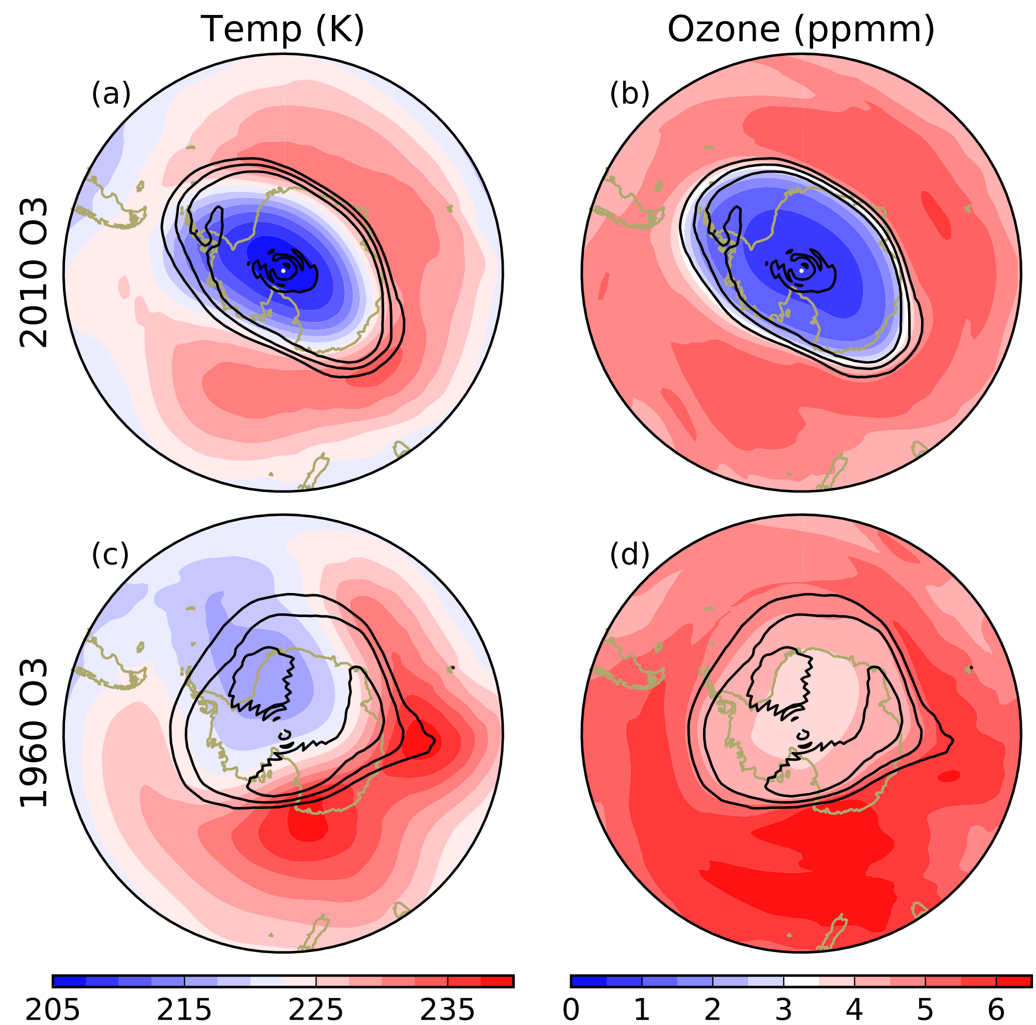

Figure 5. Snapshot of (a) temperature and (b) ozone concentration at 50 hPa from a random day in November from the *2010O3* O3Tracer simulation. (c) and (d) as in (a) and (b), except from the *1960O3* simulation. Black contours plot PV at -50, -60, and -70 PVU.

insolation is a favorable condition as the ozone-circulation interaction originates from the absorption of solar radiation by ozone. November is the optimal time for the ozone-circulation interaction to take effect given these conditions.

To quantify the effect of the ozone-circulation interaction on the radiative damping, we calculate the effective radiative damping rate following Hitchcock et al. (2010). We regress the daily radiative heating rate anomalies against temperature anomalies with zonal mean and climatological seasonal cycle removed. The resulting slope is the effective radiative damping rate, and the reciprocal of the slope is the radiative damping time scale. Figure 6 shows the regression from the three *2010O3* simulations at 60°S 50 hPa as an example. The three simulations show a similar damping rate of 0.06 day^{-1} for longwave radiation. When shortwave radiation is included, the damping rate in CNTL is not affected, but both O3Tracer and FullChem show a reduction of the radiative damping rate. This reduction comes from the shortwave absorption by the ozone anomalies that accompany the temperature anomalies. Figure 6d and 6e further show the distributions of the shortwave contribution to the radiative damping in O3Tracer and FullChem, which are generally consistent with the wave dissipation anomalies shown in Fig. 2c and 2d. Shortwave radiation leads to a reduction of the radiative damping throughout the lower stratosphere. The strongest reduction exceeding 50% is found near 50 hPa over high latitudes.

Lastly, we use an offline radiative transfer model to quantify the effect of the ozone-circulation interaction. We regress ozone anomalies upon temperature anomalies as we did with heating rates. The resulting ozone anomaly associated with 1K warming is added to the climatological mean profiles. We use Fu-Liou radiative transfer model (Fu & Liou, 1992; Rose & Charlock, 2002) to calculate the shortwave heating rate changes due to the ozone changes. The resulting heating rate changes are compared to the effective radiative damping rates from the aforementioned regression analysis. Figure 7 shows the comparison at 50 hPa. Agreement is found between the off-line radiative transfer calculation and the regression analysis. Similar agreement is also found at other levels but not shown here. The agreement between the two methods confirms that the shortwave's contribution to the radiative damping arises from the ozone anomalies associated with the temperature anomalies.

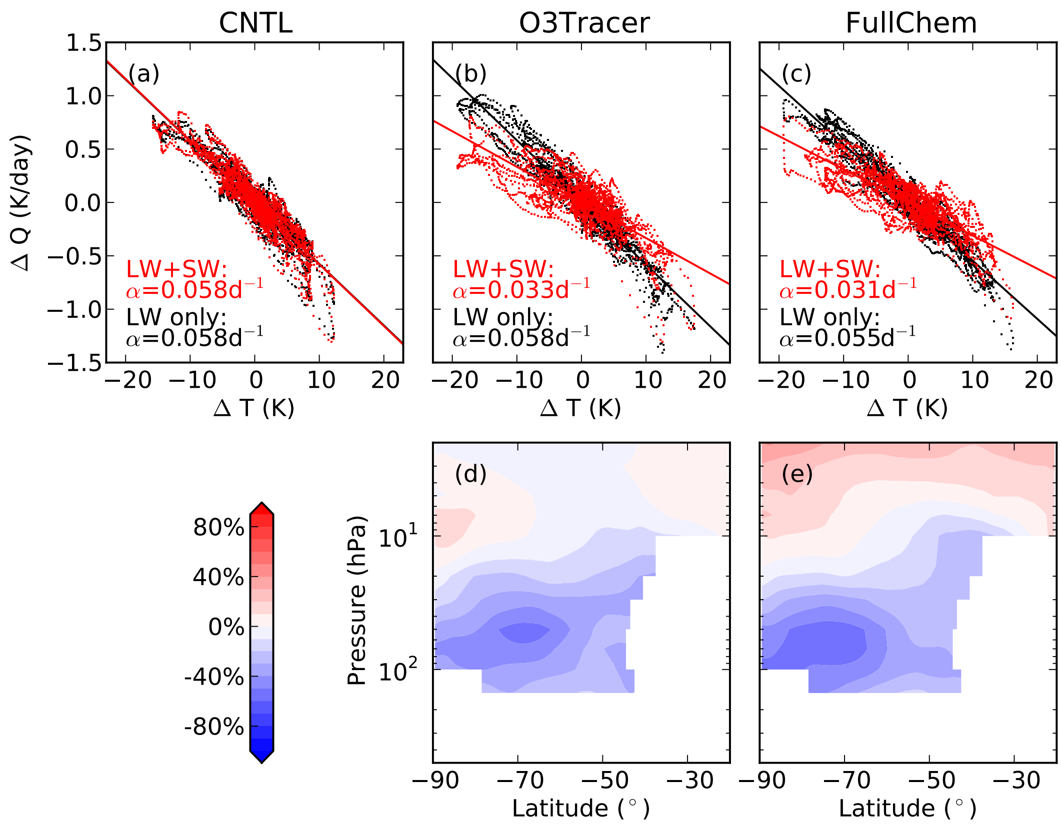

Figure 6. Scatter plot of radiative heating rate anomalies versus temperature anomalies on 15 November at 50 hPa 60°S in *2010O3* experiment from (a) CNTL, (b) O3Tracer, and (c) FullChem simulations, and relative contribution to the effective radiative damping rates from the shortwave radiation from (d) O3Tracer and (e) FullChem simulations. The anomalies are calculated by subtracting the zonal mean and the 10 year mean of the same date. For clarity, only 10 years of data are shown. Results are similar using the full length of the simulation. Black dots show the longwave (LW) radiative heating rates, and red dots show the combined heating rates from both longwave and shortwave (SW) radiation. The effective damping rate calculated from the linear orthogonal regression is listed in the legend. Relative contribution to the effective radiative damping rates from the shortwave radiation is calculated as $(\alpha_{(LW+SW)} - \alpha_{LW})/\alpha_{LW}$. Results are masked at the locations where the correlation between longwave heating rate and temperature is less than 0.7. The low correlation indicates a non-local and/or non-linear radiative damping, which is then not represented by the linear regression.

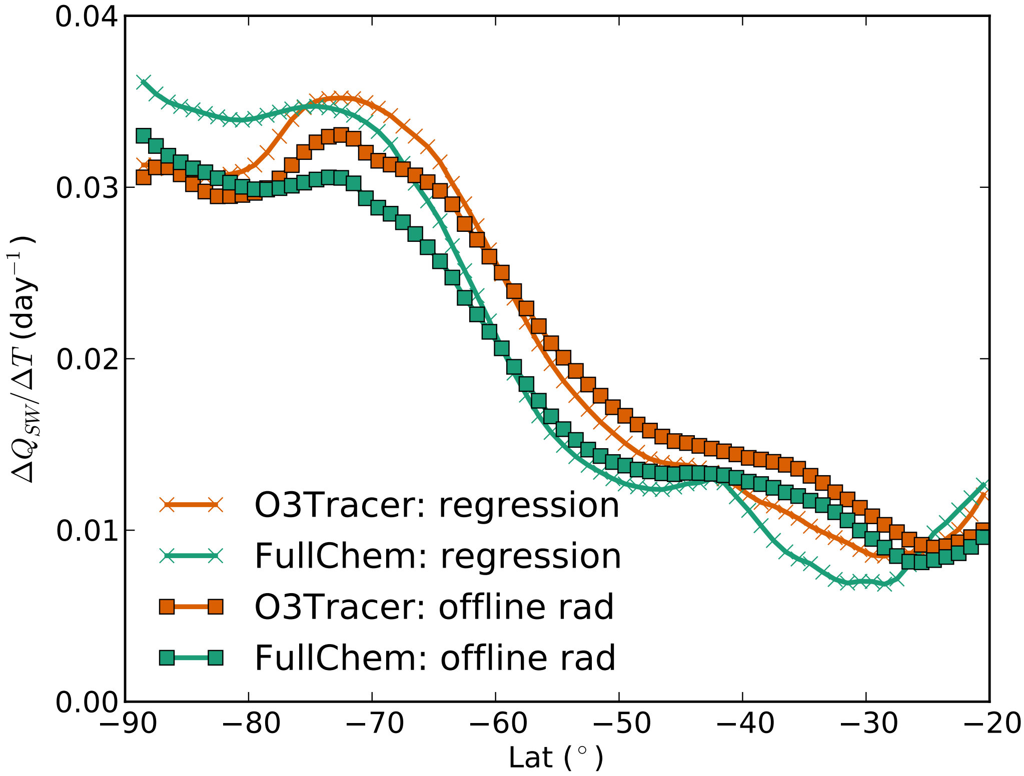

Figure 7. Shortwave heating rate associated with 1K warming at 50 hPa for November in *2010O3* simulations. Crosses indicate results from the regression between shortwave heating rate and temperature anomalies. Squares indicate results from the off-line radiative transfer calculation.

4 Summary and discussion

We simulate the climate response to stratospheric ozone depletion in GFDL AM4 with different ozone schemes: prescribing monthly zonal mean ozone concentration (CNTL), full stratospheric and tropospheric chemistry (FullChem) or prescribing monthly zonal mean chemical production rate and lifetime of ozone (O3Tracer). While similar amounts of ozone loss are produced by the three schemes, the resulting stratospheric cooling from prescribing ozone is significantly weaker than those from the other two schemes, with the largest difference occurring in November. We show that dynamics drive the difference in the stratospheric cooling. Compared to the two interactive ozone schemes, the CNTL simulation produces more wave dissipation in the lower stratosphere and less wave dissipation above, which leads to a stronger descending and dynamical warming in the polar lower stratosphere.

We identify two pathways that the dynamics respond to ozone depletion. The first one involves the strengthening of the polar vortex following the initial radiative cooling, which allows more wave dissipation in the stratosphere and enhances the dynamical heating at the polar lower stratosphere. This pathway has been well discussed in the literature (e.g., Li et al., 2008; McLandress & Shepherd, 2009; Lin et al., 2017) and is well represented in all three ozone schemes. The second pathway involves a modification of the radiative damping by ozone. With the existence of the ozone hole, large ozone anomalies co-vary with temperature anomalies. The shortwave heating from the ozone anomalies partly compensates the longwave cooling, leading to a weaker radiative damping. As a result, less wave dissipates at lower stratosphere, yielding to weaker dynamical heating over the polar region. This pathway builds on the coherence between ozone and circulation in their temporal and longitudinal variations, and hence is greatly suppressed when monthly zonal mean ozone is prescribed. On the other hand, in the two interactive ozone schemes, this second pathway does take effects and cancels with the first pathway, leading to no changes in the dynamical heating and stronger net cooling over the polar lower stratosphere

We highlight the utility of the simplified ozone scheme O3Tracer. While its computational cost is as cheap as prescribing ozone and much cheaper than FullChem, it is capable of producing a ozone hole that is as strong as the one from FullChem and is capable of representing the interaction between ozone and circulation. It is also capable of simulating the historical trend of stratospheric ozone when monthly time series of ozone production rate and lifetime are prescribed (not shown). The performance of O3Tracer degrades at the upper stratosphere and mesosphere where the coupling between the chemical reactions and the meteorology states becomes important. However, in many cases, the ozone changes in the lower stratosphere register a larger impact onto the climate system than those in the upper levels. Given the increased complexity of the climate models that are not proportional to the increase of computational resources, the simplified ozone scheme may be a more practical and efficient choice for future climate model development.

Appendix A Calculating coefficients needed for the O3Tracer scheme

Rapid reactions occur between O and O_3, and the ozone concentration is not affected much by the cycling between the two. Instead, what controls the ozone concentration is the production rate of odd oxygen Ox, the sum of O and O_3. The Ox production rates can be directly diagnosed from the FullChem simulations, which includes the photolysis of oxygen as well as various chemical reactions considered in AM4. The lifetime τ is calculated as

$$\tau = -X_{[O3]}/(P - Q),$$

where $X_{[O3]}$ is the ozone concentration, P is the Ox production rates, and Q is the net chemical tendency of ozone, all of which are outputted from the FullChem simulations. The monthly 3D fields of P and τ are then averaged zonally and averaged over the years. The resulting zonal mean monthly climatology is what the O3Tracer scheme uses.

Figure A1 shows P and τ used for the *2010O3* simulations in two representative months. As expected from the Chapman mechanism, ozone production rate generally follows the solar actinic flux, which increases with height and vanishes near the winter pole. The lifetime of ozone varies from years to minutes. Long lifetime is found in the upper troposphere and lower stratosphere, where ozone can be treated as a conservative tracer. Figure A1 also plots the difference in P and τ between the *2010O3* and *1960O3* simulations. Compared to the *1960O3* scenario, the *2010O3* case shows a modest increase of ozone production over the extratropical stratosphere and a reduction of ozone lifetime throughout the stratosphere.

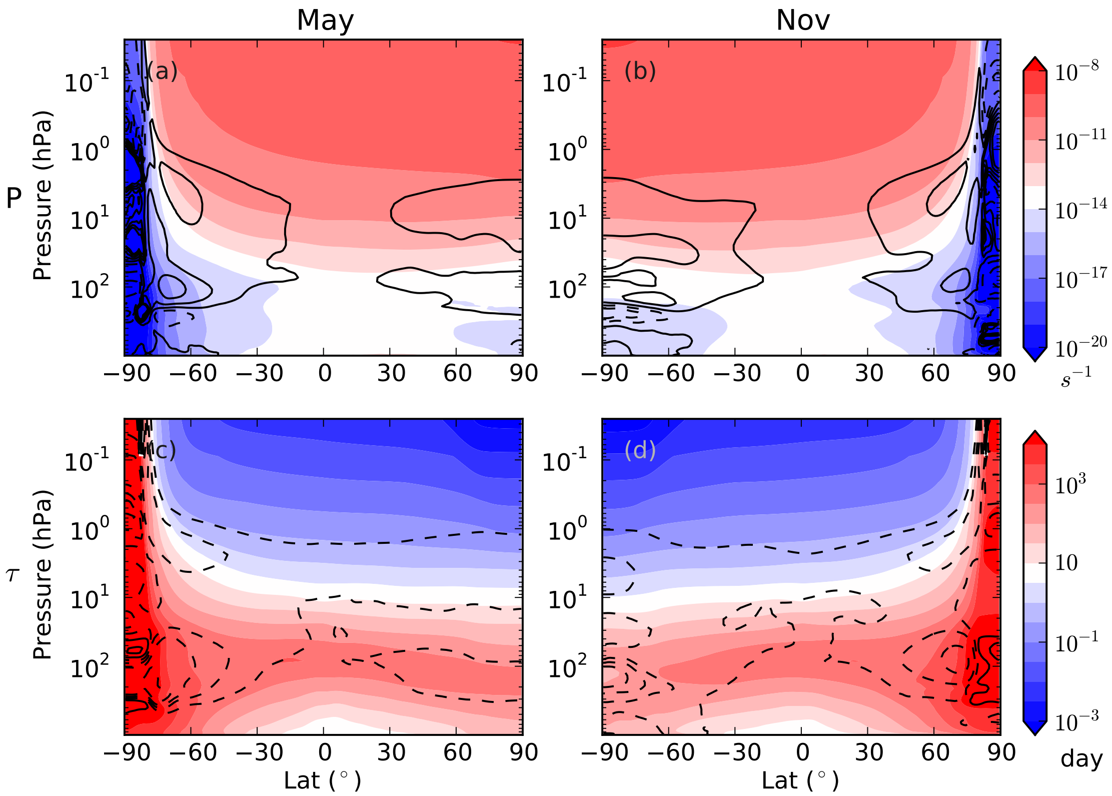

Figure A1. Coefficients used for *2010O3* O3Tracer simulations (color shading), and the relative difference between coefficients for *2010O3* and *1960O3* (contours). (a) Production rate in May. (b) Production rate in November. (c) Lifetime in May. (d) Lifetime in November. Contour intervals are −90%, −70%, ..., 70%, 90%. Negative contours are plotted in dashed lines.

Acknowledgments

We thank Larry W. Horowitz for his advice on constructing the O3Tracer scheme. This report was prepared by Pu Lin under award NA18OAR4320123 from the National Oceanic and Atmospheric Administration, U.S. Department of Commerce. The statements, findings, conclusions, and recommendations are those of the author(s) and do not necessarily reflect the views of the National Oceanic and Atmospheric Administration, or the U.S. Department of Commerce. The simulations used in the paper are permanently stored at the GFDL archive and are fully backed up. They are available upon request.The Fu-Liou radiative transfer code is provided by NASA Langley research center, available at: `https://cloudsgate2.larc.nasa.gov/cgi-bin/fuliou/lflcode/accesslfl.cgi`

References

Andrews, D. G., Holton, J. R., & Leovy, C. B. (1987). *Middle atmosphere dynamics* (Vol. 40). San Diego: Academic Press.

Austin, J., & Wilson, R. J. (2006). Ensemble simulations of the decline and recovery of stratospheric ozone. *J. Geophys. Res.*, *111*. doi: 10.1029/2005JD006907

Butchart, N. (2014). The Brewer-Dobson circulation. *Rev. Geophys.*, *52*, 157-184.

Cariolle, D., & Déqué, M. (1986). Souther Hemisphere medium-scale waves and total ozone disturbances in a spectral general circulation model. *J. Geophys. Res.*, *91*, 10825-10846.

Charney, J. G., & Drazin, P. G. (1961). Propagation of planetary scale disturbances from the lower into the upper atmosphere. *J. Geophys. Res.*, *66*, 83-109. doi: 10.1029/JZ066i001p00083

Checa-Garcia, R., Hegglin, M. I., Kinnison, D., Plummer, D. A., & Shine, K. P. (2018). Historical tropospheric and stratospheric ozone radiative forcing using the cmip6 database. *Geophys. Res. Lett.*, *45*, 3264-3273. doi: 10.1002/2017GL076770

Dunne, J. P., Horowitz, L. W., Adcroft, A. J., Ginoux, P., Held, I. M., John, J. G., … others (2020). The GFDL earth system model version 4.1 (GFDL-ESM 4.1): Overall coupled model description and simulation characteristics. *J. Adv. Model. Earth Sy.*. doi: 10.1029/2019MS002015

Eyring, V., Arblaster, J. M., Cionni, I., Sedláček, J., Perlwitz, J., Young, P. J., … Watanabe, S. (2013). Long-term ozone changes and associated climate impacts in CMIP5 simulations. *J. Geophys. Res.*, *118*, 5029-5060. doi: 10.1002/jgrd.50316

Fu, Q., & Liou, K.-N. (1992). On the correlated k-distribution method for radiative transfer in nonhomogenous atmospheres. *J. Atmos. Sci.*, *49*, 2139-2156. doi: 10.1175/1520-0469(1992)049⟨2139:OTCDMF⟩2.0.CO;2

Geer, A. J., Lahoz, W. A., Jackson, D. R., Cariolle, D., & McCormack, J. P. (2007). Evaluation of linear ozone photochemistry parameterizations in a stratosphere-troposphere data assimilation system. *Atmos. Phys. Chem.*, *7*, 939-959.

Gerber, E. P., & Son, S.-W. (2014). Quantifying the summertime response of the austral jet stream and Hadley cell to stratospheric ozone and greenhouse gases. *J. Clim.*, *27*, 5538-5559. doi: 10.1175/JCLI-D-13-00539.1

Gillett, N. P., Scinocca, J. F., Plummer, D. A., & Reader, M. C. (2009). Sensitivity of climate to dynamicallyconsistent zonal asymmetries in ozone. *Geophys. Res. Lett.*, *36*. doi: 10.1029/2009GL037246

Golaz, J.-C., Caldwell, P. M., Roekel, L. P. V., Petersen, M. R., Tang, Q., Wolfe, J. D., … others (2019). The DOE E3SM coupled model version 1: overview and evaluation at standard resolution. *J. Adv. Model. Earth Sy.*, *11*, 2089-2129. doi: 10.1029/2018MS001603

Haase, S., Fricke, J., Kruschke, T., Wahl, K., & Matthes, K. (2020). Sensitivity of the southern hemisphere circumpolar jet response to Antarctic ozone depletion: prescribed versus interactive chemistry. *Atmos. Phys. Chem.*, *20*, 14043-14061. doi: 10.5194/acp-20-14043-2020

Haase, S., & Matthes, K. (2019). The importance of interactive chemistry for stratospheretroposphere coupling. *Atmos. Phys. Chem.*, *19*, 3417-3232. doi: 10.5194/acp-19-3417-2019

Haynes, P. H., Marks, C. J., McIntyre, M. E., Shepherd, T. G., & Shine, K. P. (1991). On the downward control of extratropical diabatic circulations by eddy-induced mean zonal forces. *J. Atmos. Sci.*, *48*, 651-679.

Held, I. M., Guo, H., Adcroft, A., Dunne, J. P., Horowitz, L. W., Krasting, J., … Zadeh, N. (2019). Structure and performance of GFDL's CM4.0 climate model. *J. Adv. Model. Earth Sy.*, *11*, 3691-3727. doi: 10.1029/2019MS001829

Hitchcock, P., Shepherd, T. G., & Yoden, S. (2010). On the approximation of local and linear radiative damping in the middle atmosphere. *J. Atmos. Sci.*, *67*, 2070-2085. doi: 10.1175/2009JAS3286.1

Horowitz, L. W., Naik, V., Paulot, F., Ginoux, P. A., Dunne, J. P., Mao, J., ... Zhao, M. (2020). The GFDL global atmospheric chemistry-climate model AM4.1: model description and simulation characteristics. *J. Adv. Model. Earth Sy.*. doi: 10.1029/2019MS002032

Keeble, J., Hassler, B., Banerjee, A., Checa-Garcia, R., Chiodo, G., Davis, S., ... Wu, T. (2020). Evaluating stratospheric ozone and water vapor changes in CMIP6 models from 1850-2100. *Atmos. Phys. Chem. Disc.*. doi: 10.5194/acp-2019-1202

Li, F., Austin, J., & Wilson, J. (2008). The strength of the Brewer-Dobson circulation in a changing climate: coupled chemistry-climate model simulations. *J. Clim.*, *21*, 40-57. doi: 10.1175/2007JCLI1663.1

Li, F., Vikhliaev, Y. V., Newman, P. A., Pawson, S., Perlwitz, J., Waugh, D. W., & Douglass, A. R. (2016). Impacts of interactive stratospheric chemistry on antarctic and southern ocean climate change in the Goddard Earth Observing System, version 5 (GEOS-5). *J. Clim.*, *29*, 3199-3218.

Lin, P., Paynter, D., Polvani, L., Correa, G. J. P., Ming, Y., & Ramaswamy, V. (2017). Dependence of model-simulated response to ozone depletion on stratospheric polar vortex climatology. *Geophys. Res. Lett.*, *44*, 6391-6398. doi: 10.1002/2017GL073862

McCormack, J. P., Eckermann, S. D., coy, L., Allen, D. R., Kim, Y.-J., Hogan, T., ... Trepte, C. R. (2004). NOGAPS-ALPHA model simulations of stratospheric ozone during the SOLVE2 campaign. *Atmos. Phys. Chem.*, *4*, 2401-2423. doi: 10.5194/acp-4-2401-2004

McLandress, C., & Shepherd, T. G. (2009). Simulated anthropogenic changes in the Brewer-Dobson circulation, including its extension to high latitudes. *J. Clim.*, *22*, 1516-1540. doi: 10.1175/2008JCLI2679.1

McLinden, C. A., Olsen, S. C., Hannegan, B., Wild, O., & Prather, M. J. (2000). Stratospheric ozone in 3-d models: a simple chemistry and the cross-tropopause flux. *J. Geophys. Res.*, *105*, 14635-14665.

Michou, M., Nabat, P., Saint-Martin, D., Bock, J., Decharme, B., Mallet, M., ... Voldoire, A. (2019). Present-day and historical aerosol and ozone characteristics in CNRM CMIP6 simulations. *J. Adv. Model. Earth Sy.*, *12*. doi:

10.1029/2019MS001816

Monge-Sanz, B. M., Chipperfield, M. P., Cariolle, D., & Feng, W. (2011). Results from a new linear o_3 scheme with embedded heterogeneous chemistry compared with the parent full-chemistry 3-D CTM. *Atmos. Phys. Chem.*, *11*, 1227-1242. doi: 10.5194/acp-11-1227-2011

Neely, R. R., Marsh, D. R., Smith, K. L., Davis, S. M., & Polvani, L. M. (2014). Biases in Southern Hemisphere climate trends induced by coarsely specifying the temporal resolution of stratospheric ozone. *Geophys. Res. Lett.*, *41*, 8602-8610. doi: 10.1002/2014GL061627

Newman, P. A., & Randel, W. J. (1988). Coherent ozone-dynmical changes during the southern hemisphere spring, 1979-1986. *J. Geophys. Res.*, *93*, 12585-12606.

Polvani, L. M., Waugh, D. W., Correa, G. J. P., & Son, S. W. (2011). Stratospheric ozone depletion: the main driver of twentieth-century atmospheric circulation changes in the Southern Hemisphere. *J. Clim.*, *24*, 795-812. doi: 10.1175/2010JCLI3772.1

Rae, C. D., Keeble, J., Hitchcock, P., & Pyle, J. A. (2019). Prescribing zonally asymmetric ozone climatologies in climate models: Performance compared to a chemistry-climate model. *J. Adv. Model. Earth Sy.*, *11*, 918-933.

Rieder, H. E., Chiodo, G., Fritzer, J., Wienerroither, C., & Polvani, L. M. (2019). Is interactive ozone chemistry important to represent polar cap stratospheric temperature variability in earth-system models? *Environ. Res. Lett.*, *14*, 044026. doi: 10.1088/1748-9326/ab07ff

Rose, F. G., & Charlock, T. P. (2002). New Fu-Liou code tested with ARM Raman lidar and CERES in pre-CALIPSO exercise. In *the 11th conference on atmospheric radiation.* Ogden, Utah. (https://ams.confex.com/ams/pdfpapers/42757.pdf)

Schoeberl, M. R., & Hartmann, D. L. (1991). The dynamics of the stratospheric polar vortex and its relation to springtime ozone depletions. *Science*, *251*, 46-52. doi: 10.1126/science.251.4689.46

Solomon, S. (1999). Stratospheric ozone depletion: a review of concepts and history. *Rev. Geophys.*, *37*, 275-316. doi: 10.1029/1999RG900008

Solomon, S., Portmann, R. W., Sasaki, T., Hofmann, D. J., & Thompson, D. W. J.

(2005). Four decades of ozonesonde measurements over Antarctica. *J. Geophys. Res.*, *110*.

Son, S.-W., Gerber, E. P., Perlwitz, J., Polvani, L. M., Gillett, N. P., Seo, K.-H., ... others (2010). Impact of stratospheric ozone on Southern Hemisphere circulation change: a multimodel assessment. *J. Geophys. Res.*, *115*. doi: 10.1029/2010JD014271

Son, S.-W., Polvani, L. M., Waugh, D. W., Akiyoshi, H., Garcia, R. R., Kinnison, D., ... Shibata, K. (2008). The impact of stratospheric ozone recovery on the Southern Hemisphere westerly jet. *Science*, *320*, 1486-1489.

Voldoire, A., Sanchez-Gomez, E., y Mélia dn B. Decharme, D. S., Cassou, C., Sénési, S., Valcke, S., ... Chauvin, F. (2013). The CNRM-CM5.1 global climate model: description and basic evaluation. *Clim. Dynam.*, *40*, 2091-2121. doi: 10.1007/s00382-011-1259-y

Waugh, D. W., Oman, L., Newman, P. A., Stolarski, R. S., Pawson, S., Nielsen, J. E., & Perlwitz, J. (2009). Effect of zonal asymmetries in stratospheric oozne on simulated Southern Hemisphere climate trends. *Geophys. Res. Lett.*, *36*. doi: 10.1029/2009GL040419

Zhao, M., Golaz, J.-C., Held, I. M., Guo, H., Balaji, V., Benson, R., ... others (2018a). The GFDL global atmosphere and land model AM4.0/LM4.0: 1. simulation characteristics with prescribed ssts. *J. Adv. Model. Earth Sy.*, *10*, 691-734. doi: 10.1002/2017MS001208

Zhao, M., Golaz, J.-C., Held, I. M., Guo, H., Balaji, V., Benson, R., ... others (2018b). The GFDL global atmosphere and land model AM4.0/LM4.0: 2. model description, sensitivity studies, and tuning strategies. *J. Adv. Model. Earth Sy.*, *10*, 735-769. doi: 10.1002/2017MS001209